

Numerical simulation of semiconductor lasers

MARIUSZ ZBROSZCZYK

Institute of Electron Technology, al. Lotników 32/46, 02-668 Warszawa, Poland.

Numerical simulation based on the self-consistent solution of Poisson equation, current continuity equations, as well as on the wave equation and photon rate equation has been used to optimize lasers designs. Results of modelling for GaAs/AlGaAs, InGaAlAs/GaAs and InGaAs/GaAs quantum well lasers are presented.

1. Introduction

Numerical modelling is a very important tool for the optimization of semiconductor lasers and can significantly decrease the number of technological processes. Optical and electrical parameters, like the emitted wavelength and threshold current, should be obtained in theoretical analysis. Transport of electrons and holes in a laser is described by three differential equations: Poisson equation and continuity equations for electrons and holes. Because of complicated interactions between variables in general, only a numerical solution of these equations is possible. In this work we have used PICS3D simulation package developed by Crosslight Soft. Inc. [1].

2. Description of physical model

The basic equations used to describe the semiconductor laser behavior are Poisson's equation

$$-\nabla\left(\frac{\epsilon\epsilon_0}{e}\nabla V\right) = -n + p + N_D(1 - f_D) - N_A f_A + \sum_j N_{ij}(\delta_i - f_{ij}), \quad (1)$$

and the current continuity equations for electrons and holes:

$$\nabla J_n - \sum_j R_n^{ij} - R_{sp} - R_{st} - R_{au} = \frac{\partial n}{\partial t} + N_D \frac{\partial f_D}{\partial t}, \quad (2)$$

$$\nabla J_p - \sum_j R_p^{ij} + R_{sp} + R_{st} + R_{au} = -\frac{\partial p}{\partial t} + N_A \frac{\partial f_A}{\partial t}. \quad (3)$$

These equations govern the electrical behavior of a semiconductor laser. The current densities J_n and J_p in Eqs. (2) and (3) can be written as functions of the carrier concentration and the quasi-Fermi levels:

$$J_n = n\mu_n \nabla E_{fn}, \quad (4)$$

$$J_p = n\mu_p \nabla E_{fp} \quad (5)$$

where μ_n and μ_p are mobilities of electrons and holes, respectively.

Recombination due to deep level traps (Shockley–Read–Hall recombination) is described by:

$$R_n^{ij} = c_{nj}nN_{ij}(1 - f_{ij}) - c_{nj}n_{1j}N_{ij}f_{ij}, \quad (6)$$

$$R_p^{ij} = c_{pj}nN_{ij}(1 - f_{ij}) - c_{pj}n_{1j}N_{ij}f_{ij} \quad (7)$$

where n_{1j} is the electron concentration when the electron quasi-Fermi level coincides with the energy level E_{ij} of the j -th trap. A similar definition applies to p_{1j} . The capture coefficients c_{nj} and c_{pj} for electrons and holes relate to the lifetime of the carriers due to the j -th recombination center by the following relation:

$$\frac{1}{\tau_{nj}} = c_{nj}N_{ij}, \quad (8a)$$

$$\frac{1}{\tau_{pj}} = c_{pj}N_{ij}. \quad (8b)$$

The Auger recombination rate is given by

$$R_{au} = (C_n n + C_p p)(np - n_i^2) \quad (9)$$

where the Auger coefficients C_n and C_p depend on the type of material simulated.

Helmholtz equation must be solved to describe the optical behavior

$$\nabla^2 W + k_0^2(\epsilon - \beta^2)W = 0. \quad (10)$$

Under the scalar wave assumption, the wave equation can be solved with the technique of variable separation. We assume that the solution to the wave equation can be written as the product

$$E_\omega(x, y, z) = E_\omega(z)\phi_0(x, y) \quad (11)$$

where E_ω is the optical frequency and z is the direction along the waveguide.

The z -dependent part of the electric field $E_\omega(z)$ satisfies the equation

$$\left(\frac{\partial^2}{\partial z^2} + k^2(z) \right) E_\omega(z) = f_\omega(z) \quad (12)$$

where $f_{\omega}(z)$ is the Langevin noise function due to spontaneous emission. For an isolated semiconductor laser, the physical solution to Eq. (12) would be zero if the spontaneous noise term was absent. A simple physical explanation is that the spontaneous emission noise generates or excites the photons, which are then amplified by the presence of the optical gain. Lasing oscillation is achieved if the round trip gain approaches unity. The optical power at any bias condition is determined both by the spontaneous emission and the optical gain. The complex propagation constant $k(z)$ contains information about the solution of the transverse and lateral dimensions. The effective index and the $k(z)$ are dependent on the frequency, material properties and the photon density.

In a device simulator for optoelectronics, it is important to evaluate the carrier density and the optical gain of a quantum well. The local gain due to a transition from a conduction band labelled j to a valence band labelled i can be written as [2]:

$$g_{ij}E_{ij}^0 = \frac{2\pi}{\hbar} |H_{ij}|^2 (f_j' - f_i') \frac{\epsilon_1}{\bar{n}c} \rho_{ij}, \tag{13}$$

$$\rho_{ij} = \rho_{ij}^0 h(\hbar\omega - E_{ij}^0), \tag{14}$$

$$|H_{ij}|^2 = \left(\frac{q}{m_0}\right)^2 \frac{2\hbar\omega}{4\epsilon_1\epsilon_0\omega^2} M_{ij}^2 \tag{15}$$

where \bar{n} is the real part of the refractive index, f_i' and f_j' – the modified Fermi functions for the i -th and the j -th levels.

M_0 is the dipole momentum matrix element of the bulk material given by the following expression:

$$M_0 = \frac{m_0 E_{g0} (E_{g0} + \Delta)}{6m_e (E_{g0} + 2\Delta/3)}. \tag{16}$$

We use the following formulas for anisotropic dipole momentum matrix elements for the heavy and light hole transitions in a quantum well [3]:

$$M_{hh} = A_{hh} O_{ij} M_0, \tag{17}$$

$$M_{lh} = A_{lh} O_{ij} M_0, \tag{18}$$

$$A_{hh} = \frac{3 + 3 \cos \theta_e}{4} \quad \text{for TE}, \tag{19}$$

$$A_{lh} = \frac{5 - 3 \cos \theta_e}{4} \quad \text{for TE}, \tag{20}$$

$$A_{hh} = \frac{3 - 3 \cos \theta_e}{2} \quad \text{for TM}, \tag{21}$$

$$A_{lh} = \frac{1 + 3 \cos \theta_e}{2} \quad \text{for TM,} \quad (22)$$

where A_{nh} and A_{lh} are the quantum well dipole moment enhancement factors. Coefficient $\cos(\theta_e)$ is defined as

$$\cos \theta_e = \frac{E_{ij}^0}{E} \quad \text{for } E > E_{ij}^0, \quad (23)$$

$$\cos \theta_e = 1 \quad \text{for } E > E_{ij}^0. \quad (24)$$

In our calculations we use the TE (transverse electromagnetic) mode as the default. The TM (transverse magnetic) mode should be set if a large tensile strain is present in the material.

Ohmic contacts are implemented as simple Dirichlet boundary conditions, where the surface potential and electron and hole quasi-Fermi levels ($V_s, E_{fn}^s, E_{fp}^s, \phi_n^s, \phi_p^s$) are fixed.

The minority and majority carrier quasi-Fermi potentials are equal and set to the applied bias of the electrode

$$\phi_n^s = \phi_p^s = -E_{fn}^s = E_{fp}^s = V_{app}. \quad (25)$$

Four types of boundary conditions for the wave equation are implemented: the zero, symmetric, antisymmetric, and exponential boundary conditions. The zero boundary condition used in our simulations requires that the wave amplitude be zero along the boundary. This is a good approximation if the boundary is far enough away from the active region of the laser.

For much more detailed description of physical models used the reader is referred to the software documentation [1].

3. Description of the structures

Three types of heterostructures were analysed and the main difference is the material of the active region GaAs, InGaAs or InGaAlAs. For the heterostructures with GaAs active region the layers sequence was as follows: 1.2 μm $\text{Al}_{0.4}\text{Ga}_{0.6}\text{As}$ n-type cladding layer, 0.3 μm $\text{Al}_{0.25}\text{Ga}_{0.75}\text{As}$ waveguide layer with one or four GaAs quantum wells in the middle, and 1.2 μm $\text{Al}_{0.4}\text{Ga}_{0.6}\text{As}$ p-type cladding layer. Waveguide and quantum well regions were undoped. Cladding layers were doped to the level $5 \times 10^{17} \text{ cm}^{-3}$ and 10^{18} cm^{-3} for n-type and p-type, respectively.

The second type of laser structures consisted of 1.5 μm $\text{Al}_{0.3}\text{GaAs}$ n-type cladding layer, undoped active 80 \AA InGaAs quantum well layer enclosed by 0.3 μm GaAs waveguide layers, and 1.5 μm $\text{Al}_{0.3}\text{GaAs}$ p-type cladding layer [4]. Single and multiple quantum well structures were modelled. Two parameters were changed to obtain proper wavelength, *i.e.*, In content in the quantum well and the width of the quantum well.

The last type of the structures consisted of single $\text{In}_x(\text{Ga}_{0.75}\text{Al}_{0.25})_{1-x}\text{As}/\text{Al}_{0.25}\text{Ga}_{0.75}\text{As}$ quantum well surrounded by $\text{Al}_{0.25}\text{Ga}_{0.75}\text{As}$ waveguide layers and $\text{Al}_{0.4}\text{Ga}_{0.6}\text{As}$ cladding layers. The total waveguide thickness was equal to $0.3\ \mu\text{m}$, the cladding layer thickness was $1.2\ \mu\text{m}$ each. The individual quantum well thickness was augmented from $50\ \text{\AA}$ to $90\ \text{\AA}$ with $10\ \text{\AA}$ step. Indium content in active region varied from 20% to 29%.

The laser heterostructures with GaAs and InGaAlAs active region were optimized for 808 nm band at room temperature, suitable for pumping Nd-YAG solid state lasers, and the InGaAs heterostructures were designed for 980 nm operation at room temperature for application in erbium doped fiber amplifiers.

4. Results

The optical gain spectrum for the single quantum well AlGaAs/GaAs laser is shown in Fig. 1. Lines are drawn for different concentrations of injected electrons from $5 \times 10^{17}\ \text{cm}^{-3}$ to $5 \times 10^{18}\ \text{cm}^{-3}$. Maximum gain indicates approximate wavelength of the lasing mode. Figure 2 shows calculated emitted laser wavelength as a function of quantum well thickness. It is clear that we can obtain 808 nm only for a very thin quantum well of 15 monolayers thickness, roughly equal to $42\ \text{\AA}$. Figure 3 shows threshold current density versus well thickness for SQW SCH AlGaAs/GaAs lasers. One can expect minimum value of J_{th} for $70\ \text{\AA}$ quantum well but in this case the emitted wavelength is much longer than desired 808 nm (around 840 nm).

Typical light-current ($P-I$) characteristics of multi quantum well $\text{In}_{0.21}\text{Ga}_{0.79}\text{As}$ laser is shown in Fig. 4. Next figure (Fig.5) presents spectral characteristics for the same laser. Its design is optimized with regard to the emitted wavelength (980 nm) and the threshold current.

The final class of the devices analyzed are lasers with InGaAlAs active regions designed for operation at 808 nm. As it has been mentioned earlier, to get this

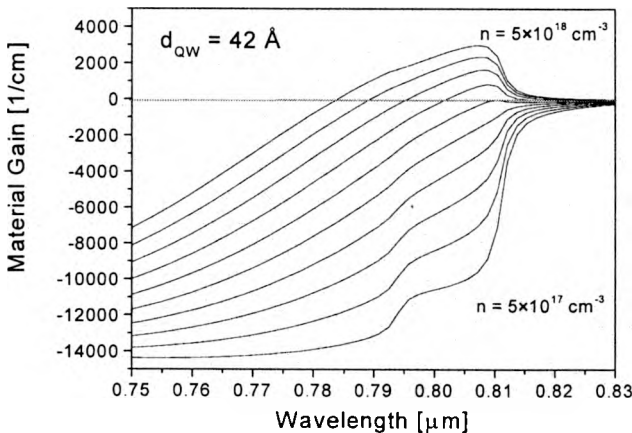


Fig. 1. Optical gain spectrum of the single quantum well AlGaAs/GaAs laser.

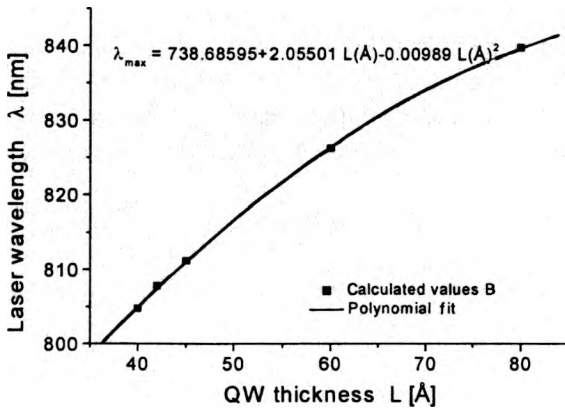


Fig. 2. Main optical mode vs. quantum well thickness of AlGaAs/GaAs single quantum well lasers.

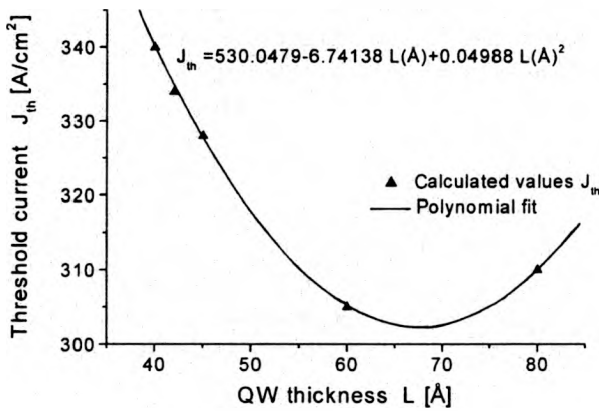


Fig. 3. Threshold current density vs. quantum well thickness of AlGaAs/GaAs single quantum well lasers.

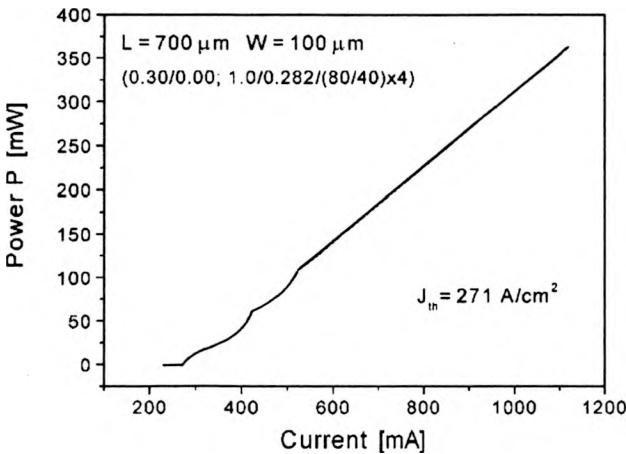


Fig. 4. Calculated light-current characteristics of the multiple quantum well $\text{In}_{0.21}\text{Ga}_{0.79}\text{As}/\text{GaAs}$ laser.

wavelength with GaAs active region we need very thin active regions, which results in poor carrier confinement and an increased threshold. Additionally, due to the discrete nature of variation of layer thickness (the effect being more pronounced in thin wells comparing to thicker ones) it is difficult, if not impossible, to obtain specified wavelength, required by the applications. The use of InGaAlAs as an active region allows for obtaining 808 nm emission wavelength with a considerably thicker quantum wells than it is in the case of GaAs. Although similar effect can be obtained with AlGaAs active region, the simultaneous addition of In stabilizes crystal lattice and makes InGaAlAs/GaAs lasers less prone to degradation.

It can be seen from Fig. 6 that there is a number of combinations of In mole fraction and the quantum well thickness which lead to lasers emitting at around 808 nm,

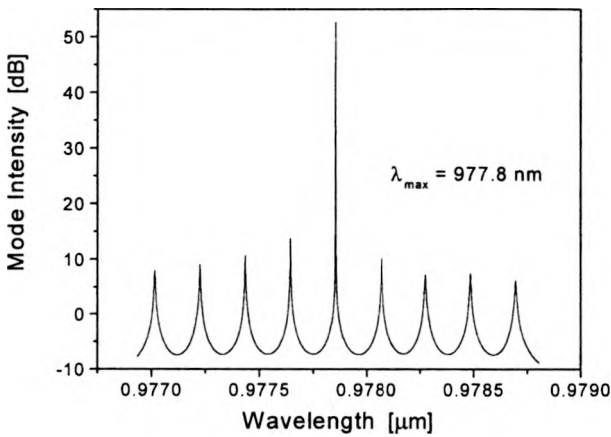


Fig. 5. Calculated spectral characteristics of the multiple quantum well $In_{0.21}Ga_{0.79}As/GaAs$ laser.

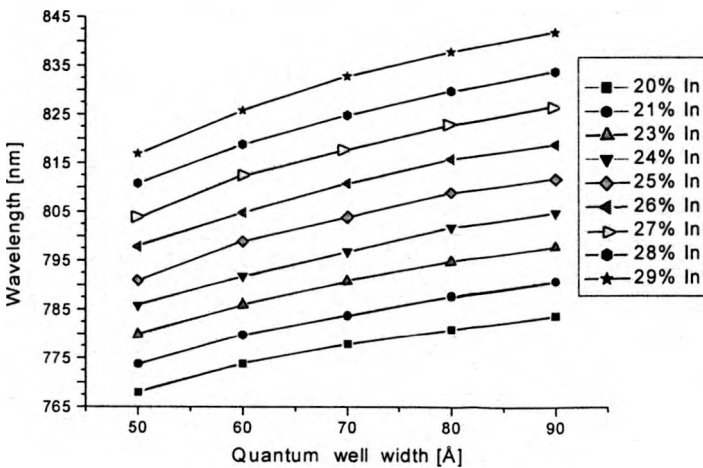


Fig. 6. Main optical mode vs. indium contents and quantum well width of InGaAlAs/GaAs single quantum well lasers.

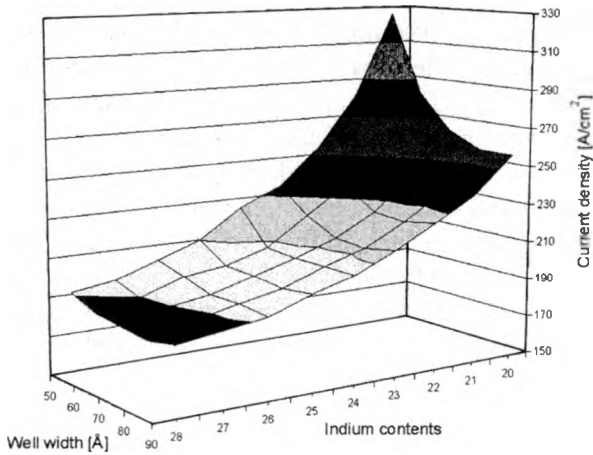


Fig. 7. Threshold current density vs. indium content and quantum well width of InGaAlAs/GaAs single quantum well lasers.

although not all of them are easily, technologically achievable due to the lattice mismatch between quantum well and barrier material, which generally increases with increasing indium content in the active region. Figure 7 shows threshold current density as a function of two variables – In content and quantum well width. From the point of view of threshold reduction, constructions with the highest technologically possible In content in the active region are desired but in practice a reasonable compromise between the threshold current and tolerable lattice mismatch has to be reached. The InGaAlAs/GaAs lasers are novel constructions, difficult from the technological point of view, but very promising as compared to standard GaAs lasers.

Acknowledgments – The author would like to thank Maciej Bugajski for helpful discussions and careful reading of the manuscript. This work was partially supported by the State Committee for Scientific Research (KBN), Poland, under grants Nos. 7T11B02121 and 8T11B07019.

References

- [1] PICS3D, Instruction Manual, Crosslight Software Inc., CA. 1998.
- [2] WOOTEN F., *Optical Properties of Solids*, Academic Press, New York. London 1972.
- [3] YAMADA M., OGITA S., YAMAGISHI M., TABATA K., IEEE. J. Quantum Electron. **21** (1985), 640.
- [4] BUGAJSKI M., REGIŃSKI K., MROZIEWICZ K., KUBICA J.M., SAJEWICZ P., PIWOŃSKI T., ZBROSZCZYK M., Opt. Appl. **31** (2001), 267.

Received May 13, 2002